Enhanced intermediate-depth nutrient import to the Late Last Interglacial Atlantic

Authors: Isaac Sipp-Alpers[1,†], Jean Lynch-Stieglitz[1], Tyler Vollmer[1], Thomas Marchitto[2]

[1]Georgia Institute of Technology, School of Earth & Atmospheric Sciences, Atlanta, GA;
[2]University of Colorado, Institute of Arctic and Alpine Research, Boulder, Colorado

[†]Corresponding Author: is9188@princeton.edu

Key Points

- Nutrient supply to the Florida Straits was high during the Late Last Interglacial due to more nutrient-rich intermediate waters
- Preformed nutrient content of intermediate waters that form in the Southern Ocean was great during the Late Last Interglacial
- High preformed nutrients in intermediate waters during the Late Last Interglacial supported significant equatorial primary productivity

Abstract

The delivery of nutrients from intermediate waters that form in the Southern Ocean is thought to be a key control on tropical ocean surface productivity. In this paper, we present geochemical evidence that an increase in low-latitude productivity during the Last Interglacial (LIG) was driven by an increase in the preformed nutrient content of Subantarctic Mode Water (SAMW). We generated records of benthic foraminiferal $\delta^{13}C$, $\delta^{18}O$, Cd/Ca and Mg/Li which are used to reconstruct seawater cadmium, dissolved oxygen, and temperature from a core site in the Florida Straits. The Florida Straits is a location of mixing between SAMW and Northern Component Water, the ratio of which is dependent on the strength of the Atlantic Meridional Overturning Circulation. We find that Late LIG seawater cadmium – which in today's ocean is correlated to phosphate – was substantially higher than the Late Holocene average at this location, while apparent oxygen utilization was similar during these two periods. Thus, we invoke higher preformed phosphate in the Florida Straits during the Late LIG relative to the Late Holocene. Increased SAMW preformed phosphate could be the result of reduced Antarctic Zone winter mixed layer residence time and greater Southern Ocean surface nutrient supply during the Late LIG compared to the Late Holocene, as supported by published reconstructions of Southern Ocean biogeochemistry and dynamics. We therefore hypothesize that higher SAMW preformed phosphate would cause an increase in the transport of nutrients into the low latitudes, thereby increasing productivity there.

1. Introduction

The equatorial oceans are among the most biologically productive regions of the modern world ocean due to the year-round availability of light at the equator and the equatorial trade winds, which drive upward mixing of nutrient-rich intermediate waters. Low-latitude productivity has implications for the development or decline of oxygen minima in the tropical subsurface ocean (Karstensen et al., 2008), as well as for seawater properties like carbonate saturation state, which in turn impacts the health of marine organisms that build calcium carbonate shells (Tyrell, 2008). A more robust understanding of the controls on equatorial productivity, itself important to our comprehension of Earth's biosphere, could also clarify the broad controls on oceanic phenomena like dysoxia.

Indeed, the annual productivity of the equatorial ocean is variable on timescales stretching from seasonal (*e.g.,* Brandt et al., 2025) to glacial-interglacial (*e.g.,* Costa et al., 2017), with different mechanisms thought to be responsible for changes in equatorial productivity at different rates, frequencies, and magnitudes. For instance, on shorter (multi-year) timescales, variability in upwelling driven by El Niño-Southern Oscillation is thought to be a chief control on nutrient delivery to the low-latitude Pacific surface ocean, and thus also modulates low-latitude productivity there (Barber & Chavez, 1986). Winckler et al. (2016) discussed the numerous hypotheses which could explain how equatorial productivity in the Pacific varied over the glacial cycles of the late Pleistocene, including theoretically stronger glacial trade wind-driven upwelling, more substantial glacial eolian Fe deposition, and changing glacial nutrient supply from the upward mixing of subsurface waters of Southern Ocean origin at the equator. Evidence from Earth system models concurs with this last point, suggesting that nutrient delivery from intermediate water masses which mix upward near the equator present a major control on equatorial productivity in the modern ocean (Sarmiento et al., 2004). Studies of past climate can help test this hypothesis and the others mentioned above by revealing how properties such as intermediate water nutrient concentrations were different in periods when low-latitude productivity was different from today. Such paleoceanographic studies are especially useful when considering past interglacial periods, where these studies can reveal the sensitivity of low-latitude productivity to intermediate water nutrient concentrations under warm climate conditions; this is relevant to the response of low-latitude productivity to modern warming.

Here we focus on the Last Interglacial Period (LIG; ca. 128,000-117,000 years ago [128-117 kyr]), which is the most recent extended period of warmth against which Holocene climate can be compared. During the LIG, Earth's climate was marginally warmer (by roughly 0.5°C-1.5°C) than the Holocene (*e.g.*, Nascimento et al., 2022; Hoffman et al., 2017; Bova et al., 2021). Atmospheric pCO_2 was very similar to the pre-Industrial Holocene (Petit et al., 1999), but orbital parameters were markedly different, with a much more eccentric orbit and lower obliquity during the LIG (Berger & Loutre, 1991). Greater primary productivity during the LIG is inferred from a number of fossil records across the equatorial world ocean (Figure 1); this change is especially obvious during the Late LIG (LLIG), which, like the Late Holocene (LH), was marginally cooler than the climate optimum it succeeded (Capron et al., 2014). With no evident change in tropical dust deposition during the LLIG relative to the LH (Skonieczny et al., 2019; Jacobel et al., 2017), we posit that the change in tropical productivity was probably driven by an increase in vertical mixing at the equator, an increase in the nutrient load of upward-mixing intermediate and deep waters, or some combination thereof.

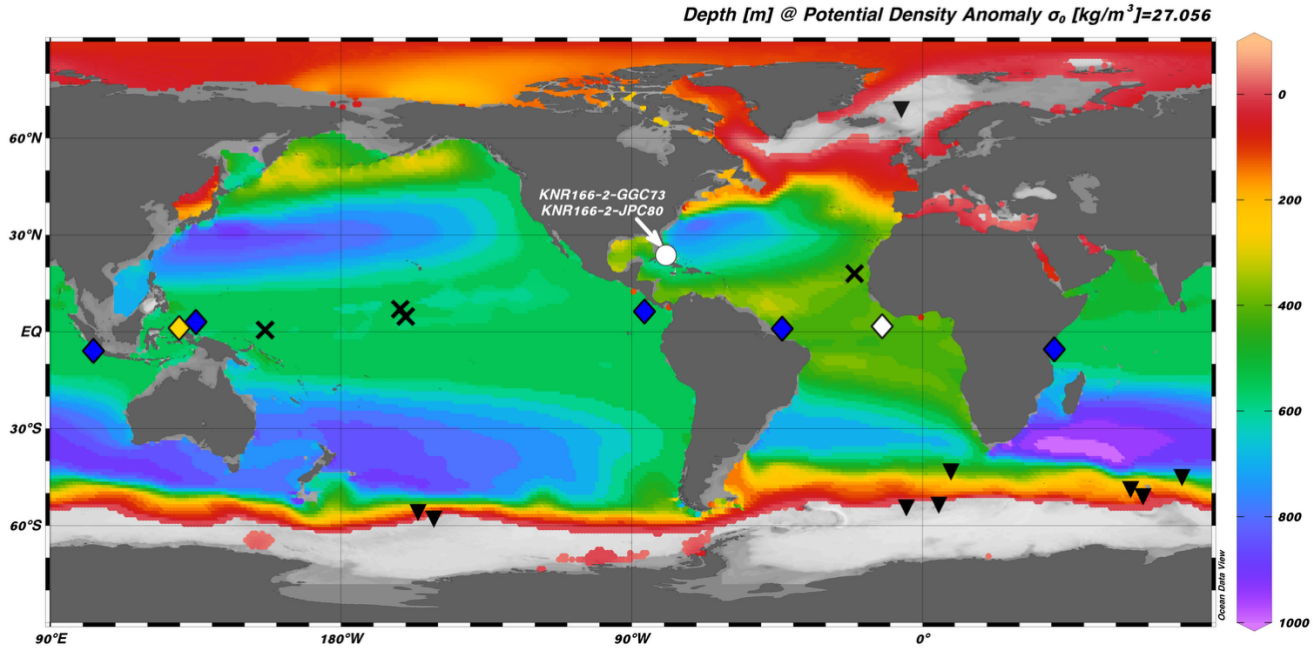

Figure 1. World map of depth along the σ_0 = 27.056 kg m^{-3} isopycnal (the isopycnal of bottom waters at the Florida Straits core site). Blue diamonds indicate equatorial core sites with higher average reconstructed productivity during the Late Last Interglacial (LLIG) than the Late Holocene (LH); from left to right: Tangunan et al. (2017), Romero et al. (2012), Kawahata et al. (1998), Marcantonio et al. (2020), Piacsek et al. (2021). The yellow diamond indicates a core site with lower average reconstructed productivity in the LLIG than the LH (Su et al., 2015) and the white diamond indicates a core site recording approximately equal productivity during these two periods (Schneider

et al., 1996). Black crosses indicate records of terrigenous dust deposition (Skonieczny et al., 2019; Jacobel et al., 2017) and inverted black triangles denote records of high-latitude ocean surface conditions we discuss (Thibodeau et al., 2017; Robinson & Sigman, 2008; Jaccard et al., 2013; Martinez-Garcia et al., 2014; Studer et al., 2015; Ai et al., 2020; Ai et al., 2024; Lamy et al., 2024). The white dot indicates the location of the cores studied herein. Figure made using Ocean Data View (Schlitzer & Reiner, 2023).

Here we introduce reconstructions of bottom-water temperature, dissolved oxygen, and seawater cadmium (which is tightly correlated with phosphate in the modern ocean; Boyle et al., 1995) from two collocal cores from the Cay Sal Bank in the Florida Straits. These cores are currently bathed by a mixture of Northern Component Water (NCW)—which we define as a mixture of predominantly Subpolar Mode Water (SPMW) along with North Atlantic Central Water and Mediterranean Water—and Subantarctic Mode Water (SAMW), the latter of which is also a major component of the intermediate waters which are thought to feed equatorial productivity in all three major ocean basins (Sarmiento et al., 2004). With these records, we seek to investigate the impact of nutrient concentration in intermediate waters on LLIG tropical productivity. Furthermore, we will deconvolve the nutrient change into its preformed and remineralized components with the goal of discerning the mechanisms which could give rise to these differences in nutrient concentration.

2. Methods

2.1 Core location and oceanographic setting

The two collocal cores examined in this study (23°44.73′ N 79°25.78′ W; 542 m modern depth) consist of a gravity core (KNR166-2-GGC73) and a piston core (KNR166-2-JPC80). A composite record is constructed using the top 396 cm of the gravity core, and depths 320 to 1050 cm in the piston core. The sections have a 76 cm overlap to enable the joining of the records to yield a single stratigraphy. We align the uppermost portion of the benthic $\delta^{18}O$ record from KNR166-2-JPC80 with that of the lowermost portion of the benthic $\delta^{18}O$ record from KNR166-2-GGC73, resulting in a downward shift of 50 cm in all sample depths in KNR166-2-JPC80 (in other words, we added 50 cm to the original depths in KNR166-2-JPC80; see Figure 2, left inset). The offset in depth between the different types of cores is likely due to compression or missing material at the top of the piston core.

Previous work on KNR166-2-GGC73 includes analyses of stable carbon and oxygen isotopes in benthic and planktonic foraminifera (Lynch-Stieglitz et al., 1999a; Lynch-Stieglitz et al., 2011) and seawater cadmium (Cd_w) and temperature (T) reconstructions using trace metal ratios in the benthic foraminifer *Hoeglundina elegans* (Lu et al., 2024). All analyses of KNR166-2-JPC80 are novel. KNR166-2-JPC80 sediment samples were wet sieved in a 63 μm sieve with deionized water and the >63 μm fraction was then dried in a 60°C oven.

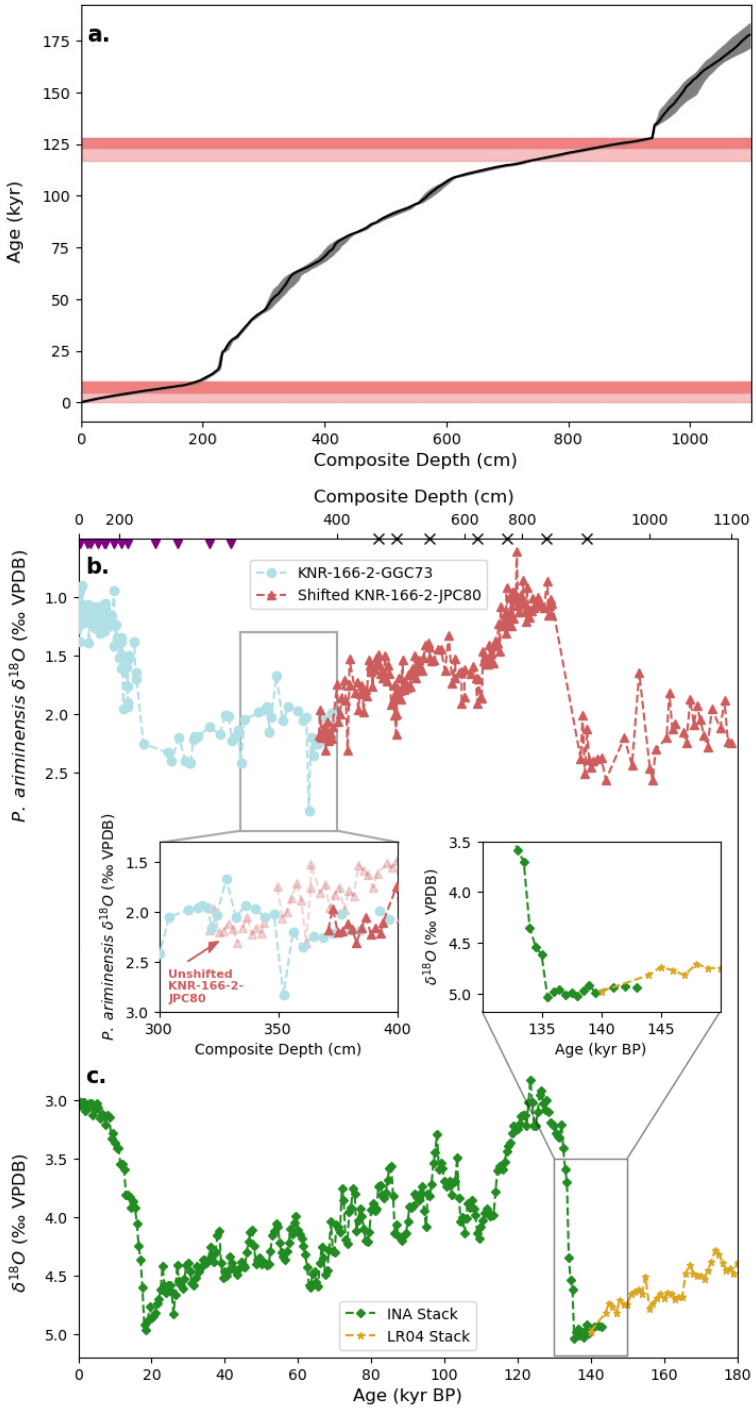

Figure 2. (**a.**) The age model developed with BIGMACS (in age vs. depth space), with climate optima (peak interglacials) highlighted in dark red and cooler periods within each interglacial highlighted in light red (according to the limits described by Ezat et al., 2024, and Marcott et al., 2013). The grey envelope denotes the 1σ error on the age model. (**b.**) Downcore composite record of *P. ariminensis* $\delta^{18}O$ for KNR166-2-GGC73 and KNR166-2-JPC80. Note that the records are plotted vs Age (bottom axis), and the top axis for depth is non-linear and corresponds to the age model shown in panel a. Purple inverted triangles on the top axis indicate depths for which the age model is

substantiated by radiocarbon measurements while black crosses indicate prescribed age-depth ties (Table A). (**c.**) Combined Intermediate North Atlantic (INA; Lisiecki & Stern, 2016) and LR04 (Lisiecki & Raymo, 2005) benthic $\delta^{18}O$ stacks used to develop our age model. Inset figures describe overlap regions for (left) KNR166-2-GGC73 and KNR166-2-JPC80, with and without the 50 cm shift applied to KNR166-2-JPC80; and (right) INA and LR04 stacks.

2.2. Measurements of stable isotopes of carbon and oxygen

Benthic foraminifera *Planulina ariminensis*, *Hoeglundina elegans*, and *Globobulimina spp.* were picked from the >250 μm size fraction of the entire composite core (hereafter KNR166-2-GGC73/JPC80). Stable oxygen and carbon isotopic ratio data ($\delta^{18}O$ and $\delta^{13}C$, respectively) for all samples of *P. ariminensis* and 51 out of 70 total samples of *Globobulimina spp.* were acquired using a Thermo MAT 253 with Kiel carbonate preparation device at the Georgia Institute of Technology (GT). Data for 19 replicate samples of *Globobulimina spp.* were acquired using a Thermo MAT 253 stable isotope mass spectrometer with Kiel carbonate preparation device at the University of Arizona (UA). At each sample depth, one to three *P. ariminensis* tests and up to five *Globobulimina spp.* tests were analyzed singly. Along with the sample analytes, NIST NBS-18 and NBS-19 carbonate standards were tested to track variability between sets of samples and an in-house Carrara marble standard at GT (IAEA-603 was the in-house standard at UA) to track variability within each individual set of samples. Analytical precision for runs with samples below 50 μg ranges from 0.021‰ to 0.080‰ for $\delta^{18}O$ and 0.016‰ to 0.050‰ for $\delta^{13}C$. Analytical precision for samples above 50 μg ranges from 0.028‰ to 0.055‰ for $\delta^{18}O$ and 0.011‰ to 0.029‰ for $\delta^{13}C$. Seven samples that had either *P. ariminensis* $\delta^{18}O$ or $\delta^{13}C$ exceeding 2 population standard deviations of a 5-point running median were excluded from further analysis (including all calculations and figures), in addition to 1 sample of *Globobulimina spp.*, which constituted an outlier in both $\delta^{18}O$ and $\delta^{13}C$. See Table S1 for excluded data points.

2.3. Age model development

The BIGMACS MATLAB package (Lee et al., 2023) was used to construct an age model for the composite core. Specifically, this software was used to fit the *P. ariminensis* $\delta^{18}O$ record from KNR166-2-GGC73/JPC80 and previously-developed radiocarbon dates for KNR166-2-GGC73 (Lynch-Stieglitz et al., 2009) to an Intermediate North Atlantic (INA) stack melded with the LR04 benthic stack. The two stacks were fused in Marine Isotope Stage (MIS) 6 (Figure 2b.)

as the relevant INA benthic $\delta^{18}O$ stack is 150 kyr long, but magnetic susceptibility and *P. ariminensis* $\delta^{18}O$ trends for KNR166-2-JPC80 suggest this core could capture up to MIS 6e, which ended approximately 180 kyr before present (BP). As such, the fact that this age model is based on two, spliced stacks only affects data older than 140 kyr (in other words, the age model from the Holocene through the LIG is solely based on the INA stack). The parameters we input include a maximum allowable sedimentation rate of 20 cm/kyr (as suggested by the magnetic susceptibility record for this core) and a minimum allowable sedimentation rate of 0.125 cm/kyr (as necessitated by the hiatuses apparent in the record during the last two glacial terminations; see *Results*). 7 age-depth ties were prescribed upon visual inspection of the *P. ariminensis* $\delta^{18}O$ record. See Table A for fixed age-depth ties and their corresponding features in the isotope record. Following Ezat et al. (2024), we define the Last Interglacial as the period between 117 kyr BP and 128 kyr BP and divide it into the Early Last Interglacial (ELIG; 128-123.5 kyr BP) and the Late Last Interglacial (LLIG; 123.5-117 kyr BP). Similarly, we define the Holocene as the period from 10 kyr BP to the present and divide it into the Early Holocene (EH; 10-5 kyr BP) and the Late Holocene (LH; 5 kyr BP to the present) after Marcott et al. (2013). The average 1σ error for our entire age model is ±1.23 kyr, and this average error shrinks to ±0.25 kyr for LIG samples.

Table A. Prescribed ties between age and depth used for age model development, as inferred from the *P. ariminensis* $\delta^{18}O$ record.

Composite Depth (cm)	Age prescribed (kyr BP)	Feature
449.75	82	MIS 5a Peak
489.75	87	MIS 5b Peak
549.75	96	MIS 5c Peak
613.75	109	MIS 5d Peak
737.75	117	MIS 5e Termination
937.75	128	MIS 5e Onset
941.75	139	TII Hiatus Onset

2.4. Measurements of trace metals

The ratio of cadmium to calcium (Cd/Ca) in the benthic foraminifer *Hoeglundina elegans* from KNR166-2-GGC73/JPC80 was measured by first crushing and reductively and oxidatively cleaning the samples following Boyle and Rosenthal (1996), and then using a Thermo Finnigan Element2 Magnetic Sector Inductively Coupled Plasma-Mass Spectrometer at the Institute of Alpine and Arctic Research, University of Colorado, Boulder (INSTAAR) according to the methods of Marchitto (2006). The ratios of magnesium and lithium to calcium (Mg/Ca and Li/Ca, respectively) in *H. elegans* from KNR166-2-GGC73/JPC80 were also measured at INSTAAR and were used to calculate the ratio of magnesium to lithium (Mg/Li). With *H. elegans* Mg/Li, past bottom-water T was estimated according to the polynomial calibration, shown in Equation 1, that Marchitto et al. (2018) proposed:

$$(1)\ \frac{Mg}{Li} = 0.150 + 0.0209 * T - 0.0002 * T$$

At each sample depth, one to twelve *H. elegans* fossils were analyzed together. *H. elegans* Cd/Ca data previously gathered at Woods Hole Oceanographic Institution (WHOI) (Lu et al., 2024) were corrected to the data generated at INSTAAR with the offsets calculated by Oppo et al. (2023), with Equation 2:

$$(2)\ (\frac{Cd}{Ca})_{INSTAAR} = (\frac{Cd}{Ca})_{WHOI} * 0.9863$$

Roughly two-thirds (n = 42) of the displayed trace metal data for KNR166-2-GGC73 were developed at WHOI (Lu et al., 2024), and the remainder (n = 20) at INSTAAR. Analytical precision for Cd/Ca is ±2% (1σ) based on consistency standards. In order to ensure data quality, 26 Mg/Li datapoints and 13 Cd/Ca datapoints from the full composite core (comprised of 216 measurements each of Mg/Li and Cd/Ca) are excluded from figures and calculations according to the following criteria: all samples with less than 5 μg $CaCO_3$ were discarded, in addition to Mg/Li datapoints calculated from Li/Ca or Mg/Ca outliers (Li/Ca above 6 μmol kg^{-1} or below 3 μmol kg^{-1}; Mg/Ca above 2.5 mmol kg^{-1}), Cd/Ca outliers (above 0.1 μmol kg^{-1}), T reconstructions >4° C above a 5-point running mean, and Cd_w reconstructions 2 population standard deviations away from a 5-point running mean. These excluded data are tabulated in Table S1.

2.5. Estimation of dissolved oxygen

We reconstruct dissolved oxygen concentration ($[O_2]$) using the calibration proposed by Hoogakker et al. (2025). This relationship, shown in Equation 3, yields bottom water $[O_2]$ as a function of the gradient in $\delta^{13}C$ ($\Delta\delta^{13}C$) between the epibenthic foraminifer *Cibicidoides wuellerstorfi* and the infaunal foraminifer *Globobulimina* spp. (Hoogakker et al., 2025):

$$(3)\ \ \Delta\delta^{13}C = 0.011 * [O_2] + 0.093$$

The epibenthic foraminifer *Cibicidoides wuellerstorfi* resides at the sediment-water interface and thus draws the carbon it incorporates to construct its carbonate test directly from dissolved inorganic carbon (DIC) in the bottom-water (Lutze & Thiel, 1989). *Globobulimina* spp. resides at the oxic/anoxic boundary in the sediment (Hoogakker et al., 2015), so it is assumed that all respiration between *C. wuellerstorfi* and *Globobulimina* spp. is aerobic. Aerobic respiration in the sediment between these benthic foraminifera releases isotopically light DIC into the interstitial fluid, which is eventually utilized by *Globobulimina* spp. to calcify, hence the lower $\delta^{13}C$ observed for *Globobulimina* spp. than *C. wuellerstorfi* (Figure 3b.). The change in porewater DIC between the habitats of *C. wuellerstorfi* and *Globobulimina* spp. is roughly linearly related to the amount of oxygen in the bottom-water (Equation 3), with a reported R^2 correlation of 0.78 (Vollmer et al., 2022). While this calibration was originally created using the epifaunal foraminifer *C. wuellerstorfi*, this species is not present in sufficient mass throughout the studied sediment cores. *P. ariminensis* is plentiful in these sediment cores and, like *C. wuellerstorfi*, has been shown to be an elevated foraminifer that also accurately reflects seawater $\delta^{13}C$ (Lutze & Thiel, 1989; Slowey & Curry, 1995). Following a previous study in the region (Lynch-Stieglitz et al., 2024), here we use *P. ariminensis* instead of *C. wuellerstorfi* when calculating $\Delta\delta^{13}C$.

Previous studies suggest the $\Delta\delta^{13}C$ proxy may be confounded by processes such as anaerobic respiration occurring in the sediment above the habitat depth of *Globobulimina* spp. Several species of *Globobulimina* spp. have been shown to denitrify (Nomaki et al., 2015), meaning they could conceivably reside below the sedimentary oxic/anoxic boundary. In this case, sulfate and nitrate reduction above the calcification habitat of *Globobulimina* spp. would release low-$\delta^{13}C$ DIC into the porewaters occupied by *Globobulimina* spp. without impacting [O_2], thus weakening the correlation between bottom water oxygenation and $\Delta\delta^{13}C$. Hoogakker et al. (2025) discussed this possible hindrance to the proxy and remark that as yet no evidence indicates that this is a behavior demonstrated by *Globobulimina* spp. Sedimentary carbonate dissolution could also affect $\delta^{13}C$ of porewater DIC independently of [O_2], but the waters overlying the studied core site demonstrate a calcite saturation state of 70 (Bryan & Marchitto, 2008), so we do not consider this a significant hindrance to using the $\Delta\delta^{13}C$ proxy.

At one point during MIS 6 (at composite depth 997.75 cm), *P. ariminensis* $\delta^{18}O$ was an outlier, so *P. ariminensis* $\delta^{18}O$ and $\delta^{13}C$ were excluded. Because there was still a *Globobulimina* $\delta^{13}C$ measurement at this point, we used an average of the *P. ariminensis* $\delta^{13}C$ of one sample immediately above and below the excluded point in the oxygen calculation. This datapoint is dated to MIS 6 and does not impact our conclusions related to the LLIG.

2.6 Calculation of Cd_w, phosphate, and apparent oxygen utilization

Dissolved cadmium has a labile nutrient-like profile in seawater, with low values in warm surface waters and higher concentrations in the deep ocean (Boyle et al., 1976). Seawater cadmium concentration has been shown to correlate closely with phosphate concentration, with a slightly nonlinear relationship (Elderfield & Rickaby, 2000; Middag et al., 2018; Roshan and DeVries, 2021). The curvature of this relationship, with lower seawater Cd/P at low [PO_4^{3-}], appears to be related to regional differences in the Cd/P of phytoplankton and its subsequent remineralization. If those ratios were different during the past, we might expect slight changes in the seawater Cd/P curvature, leading to minor errors in reconstructed P. Of potentially greater importance, Cd has been shown to be removed by CdS precipitation in anoxic sediments, impacting the global seawater Cd budget and theoretically affecting global ocean Cd/P. The impact of glacial/interglacial oscillations in the extent of anoxic sediments would be muted by the relatively long oceanic residence time of Cd (tens of kyr; Little et al., 2015). We have no reason to suspect a long-term trend in ocean anoxia that would cause whole ocean Cd to drift from MIS 5e toward the present.

Seawater Cd concentration has also been shown to be recorded by the ratio of cadmium to calcium in benthic foraminiferal carbonate (*e.g.,* Boyle, 1992). The benthic species *Hoeglundina elegans* incorporates Cd and Ca into its aragonitic test in a similar ratio to the contemporary local seawater Cd/Ca (a partition coefficient of 1; Boyle et al., 1995). Some evidence from calcitic benthic foraminifera suggests that Cd/Ca partition coefficients are reduced in waters that are undersaturated with respect to calcite (McCorkle et al., 1995; Marchitto et al., 2005). However, as stated, the waters bathing the core site studied herein are highly supersaturated today (calcite saturation state is 70, aragonite saturation state is 44; Bryan & Marchitto, 2008), so dissolution is not a major concern for Cd/Ca. *H. elegans* is also immune to the manganese carbonate overgrowths that can lead to diagenetically elevated Cd/Ca in calcitic foraminifera (Boyle, 1983). This makes *H. elegans* Cd/Ca an effective tool for reconstructing past seawater Cd/Ca and, by extension, past seawater [PO_4^{3-}], with demonstrated success in the Florida Straits and Bahama Banks (*e.g.,* Marchitto et al., 1998; Bryan and Marchitto, 2010; Vollmer et al., 2022; Lynch-Stieglitz et al., 2024; Valley et al., 2019; Valley et al., 2017).

To calculate seawater cadmium concentration (Cd_w), benthic Cd/Ca (μmol mol^{-1}) was first converted to seawater Cd/Ca according to Equation 4:

$$(4)\ D_{Cd} = \frac{\frac{Cd_{foram}}{Ca_{foram}}}{\frac{Cd_w}{Ca_w}}$$

where D_{Cd}, the empirical partition coefficient, described above, is assumed to be 1 for *H. elegans* (Boyle et al., 1995), and seawater calcium concentration (Ca_w) is conventionally assumed to 0.01 mol kg^{-1} (Boyle, 1992). With the Cd_w trend (Figure 3c.), past phosphate concentration ($[PO_4^{3-}]$) was calculated using the equation from Vollmer et al. (2022):

$$(5)\ \ [PO_4^{3-}] = \frac{3.3\ \mu mol\ kg^{-1}}{\left[\left(\frac{1.2\ nmol\ kg^{-1}}{Cd_w} - 1\right) * \alpha^{-1}\right] + 1}$$

where α = 2.5 for the Atlantic Ocean (Elderfield and Rickaby, 2000). The 1σ error for this calculation is 0.3 μmol kg^{-1} (Vollmer et al., 2022).

Oxygen saturation was calculated using the Gibbs SeaWater Oceanographic Toolbox, assuming no change in upper ocean salinity during the LLIG relative to the LH. AOU was calculated according to Equation 6:

$$(6)\ AOU = [O_2]_{sat} - [O_2]_{measured}$$

where $[O_2]_{sat}$ is the saturation oxygen concentration and $[O_2]_{measured}$ is the value yielded by the $\Delta\delta^{13}C$ proxy. Error for AOU is the product of compounding errors in the $\Delta\delta^{13}C$ proxy (1σ ≈ 20 μmol kg^{-1}) and the T proxy on which $[O_2]_{sat}$ is based (1σ = 1.3° C; Marchitto et al., 2018), and we estimate 1σ error for AOU to be about 34.3 μmol kg^{-1}.

To calculate remineralized phosphate (P_{remin}), we multiply the derived AOU by the Redfield ratio for $P:O_2$, which we assume to be 1:-170 (Anderson & Sarmiento, 1994) and constant over time. The approximation of P_{remin} using AOU is under some scrutiny due to its assumption of

oxygen saturation upon water mass formation, when in reality many water masses of high latitude origin form while undersaturated with respect to oxygen due to upward mixing of oxygen-poor thermocline waters and surface heat flux (Ito et al., 2004). So, our estimate for P_{remin} serves as an upper bound for this value. The estimate for P_{remin} is combined with estimates of seawater $[PO_4^{3-}]$ to deconvolve the changes in remineralized and preformed fractions from the seawater nutrient record we developed (see *Discussion*).

3. Results

Largely, our results follow expected trends across glacial-interglacial boundaries (Figure 3). The magnitude of change in *P. ariminensis* $\delta^{13}C$ from the onset of MIS 5e to the end of MIS 5e is consistent with other records from the intermediate depth North Atlantic (*e.g.*, the INA $\delta^{13}C$ stack; Lisiecki et al., 2010), and the same is true for MIS 1 (Figure 3b.). This consistency is weaker but still clear for MIS 2-5a, with the greatest deviation from our record and the stack being clear during full glacial periods MIS 2 and 6. As expected from previous work in the Florida Straits, Cd/Ca is lower in glacial periods than in interglacial periods, owing to the shift in Florida Straits mixing ratios caused by a weakening AMOC that results in a greater volume of low-nutrient NCW bathing the core site in colder periods (Valley et al, 2017).

Our coretop reconstructions of T (Figure 4a.), $[PO_4^{3-}]$ (Figure 4b.), and $[O_2]$ (Figure 4c.) strengthen confidence in our records as they show good agreement with measurements of modern seawater: the modern bottom-water T at this coresite is 10.8° C (Bryan and Marchitto, 2010), which falls within the 68% confidence interval, 10.9 ± 1.4° C, of our uppermost Mg/Li-based T estimate; the modern bottom-water $[PO_4^{3-}]$ at this coresite is approximately 1.49 μmol kg^{-1}, which falls within the 68% confidence interval, 1.19 ± 0.3 μmol kg^{-1}, of our uppermost Cd/Ca-based $[PO_4^{3-}]$ estimate; and the modern bottom-water $[O_2]$ at this core site is approximately 150 μmol kg^{-1}, which falls within the 68% confidence interval, 133 ± 19.9 μmol kg^{-1}, of our uppermost $\Delta\delta^{13}C$-based $[O_2]$ estimate. Because our records comprise the longest record of intermediate-depth Atlantic Cd_w that we are aware of, there unfortunately is no reference point against which we can compare our Last Interglacial data to evaluate its accuracy.

There is an apparent hiatus in the core during the penultimate deglaciation (TII), as inferred from the sharp jump in *P. ariminensis* $\delta^{18}O$ and an analogous event during the last

deglaciation, where the hiatus is constrained by radiocarbon dates (Lynch-Stieglitz et al., 2009; Figure 2b. herein). It is not immediately clear how much time is missing from the record for the deeper hiatus, but the roughly 0.3‰ decline in $\delta^{18}O$ between 1049.75 cm and 1053.75 cm (Figure 2b.) that is characteristic of the MIS 6c/6d boundary (Figure 2c.) indicates that the portion of the core below the hiatus is likely to be MIS 6. Because the record does not resolve the steady increase in $\delta^{18}O$ directly before the penultimate deglaciation that benthic stacks describe (see Figure 2, right inset), but it does resolve a flat $\delta^{18}O$ signature characteristic of MIS 6b immediately before the deglaciation, we posit that the hiatus includes both part of the penultimate deglaciation and MIS 6a (Sun & An, 2005), with approximately 10 kyr lost from the record.

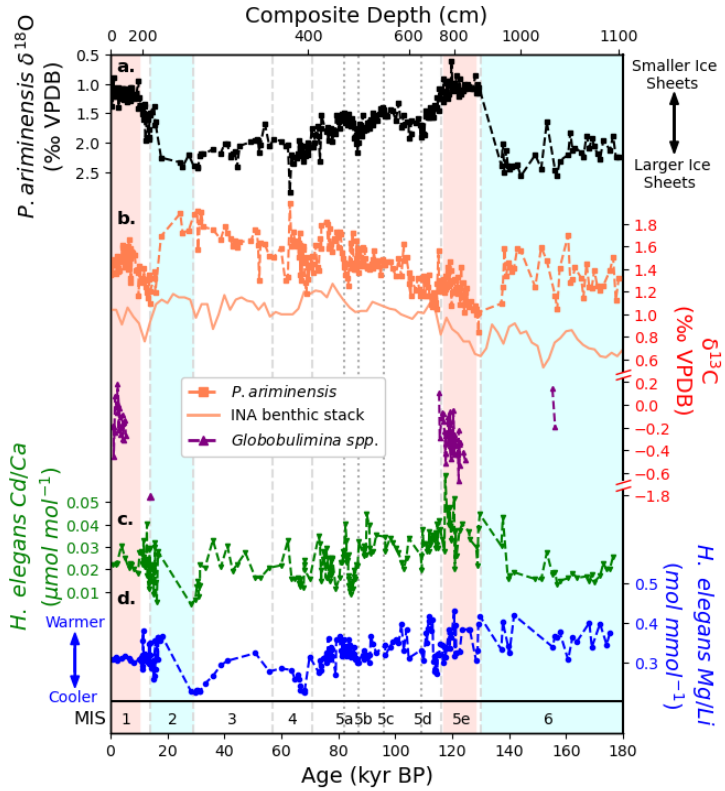

Figure 3. Results from the composite of cores KNR166-2-GGC73 and KNR166-2-JPC80. (**a.**) $\delta^{18}O$ of *Planulina ariminensis*. (**b.**) $\delta^{13}C$ of *P. ariminensis* (orange squares), the INA benthic $\delta^{13}C$ stack (light orange solid line; Lisiecki et al., 2010), and *Globobulimina spp.* (purple triangles). (**c.**) Cd/Ca of *H. elegans*. (**d.**) Mg/Li of *H. elegans*. Top (non-linear) *x*-axis denotes depth in the sediment cores and bottom *x*-axis denotes age before the present. Red shading designates full interglacial (sub)intervals, Marine Isotope Stages 1 and 5e, while blue shading designates full glacial intervals, MIS 2 and 6. Vertical, dashed lines denote boundaries of Marine Isotope Stages, which are labeled at the bottom of the figure. Vertical dotted lines denote the peaks of the subintervals of MIS 5

(Lisiecki & Raymo, 2005), also labeled at the bottom of the figure. Note the breaks in the $\delta^{13}C$ axis in (**b.**). All replicate samples are plotted.

During the LLIG, Cd_w (n = 10) was approximately 61% greater than the LH average (n = 4) (Figure 4, b. & f.), with an absolute change of about 0.149 nmol kg^{-1}. This corresponds to an increase of 0.53 µmol kg^{-1} in [PO_4^{3-}] from the LH to the LLIG (see *Methods*). Average LLIG [O_2] (n = 39) was about 9% lower than the LH average (n = 17) (Figure 4, c. & g.), with an absolute change of about 13.0 µmol kg^{-1}.

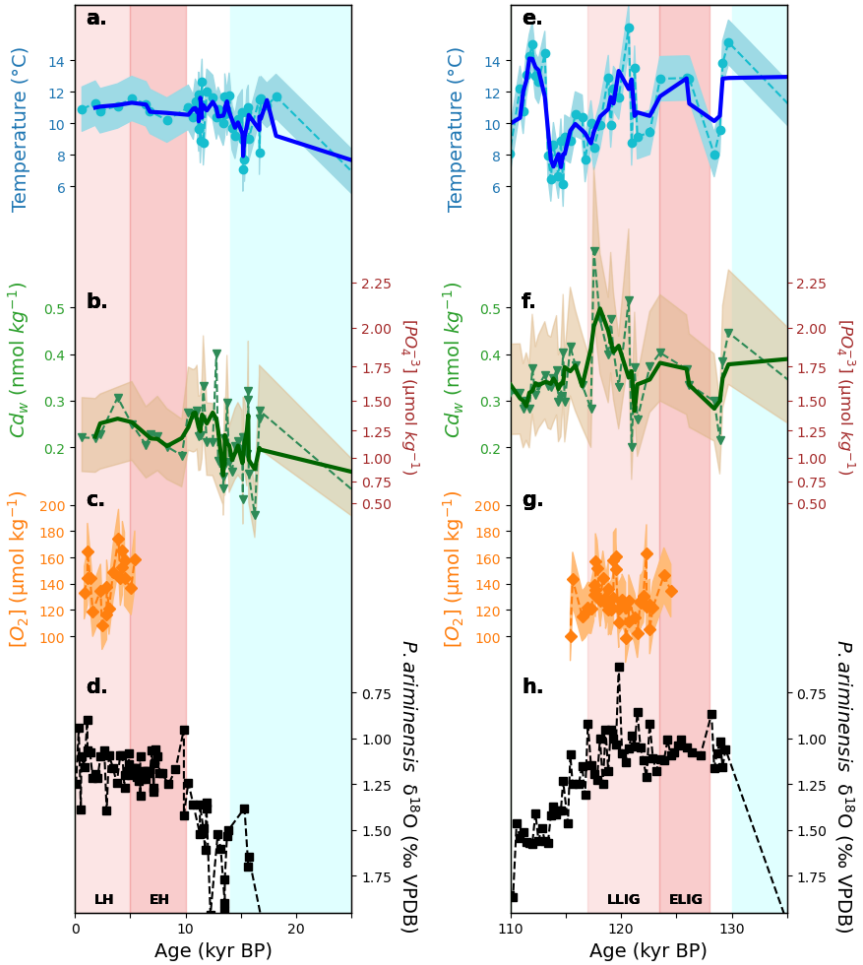

Figure 4. Comparison of trends for the period 0-25 kyr BP and 110-135 kyr BP of (**a.**, **e.**) Mg/Li-derived temperature, in degrees Celsius (°C; blue circles); (**b., f.**) seawater cadmium concentration with secondary, non-linear axis depicting seawater phosphate estimate (Elderfield & Rickaby, 2000; inverted green triangles); (**c.**, **g.**) estimated seawater oxygen concentration (orange diamonds); and (**d.**, **h.**) *P. ariminensis* $\delta^{18}O$ (black squares). Dark red shading indicates climate optima within peak interglacial periods and light red shading indicates cooler portions of peak interglacial periods, all of which are labeled at the bottom of the figure. Light blue shading indicates full

glacial periods. In all subfigures, dashed lines connect consecutive raw datapoints; solid, dark lines signify a centered, three-point running mean (where applicable); and light shading signifies the 1σ error of the calibration (where applicable). Note that the beige shading in (**b.**) and (**f.**) shows the 1σ error of the conversion from Cd_w to $[PO_4^{3-}]$. Also, note that the linear O_2 axis in (**c.**) and (**g.**) is approximately scaled to the non-linear axis for $[PO_4^{3-}]$ in (**b.**) and (**f.**) according to the assumed Redfield Ratio for these species. LH = Late Holocene; EH = Early Holocene; LLIG = Late Last Interglacial; ELIG = Early Last Interglacial.

4. Discussion

A number of factors could have contributed independently to the observed enrichment of Cd during the Late LIG. In sections *4.1 – 4.4*, we discuss four hypotheses to explain this observation: an increase in upward mixing of high-nutrient abyssal waters, an increase in remineralization in the water masses bathing KNR166-2-GGC73/JPC80, a change in AMOC strength which would directly impact Florida Straits isopycnal tilt (Lynch-Stieglitz et al., 1994), and a change in preformed nutrient concentration of the water masses bathing KNR166-2-GGC73/JPC80.

4.1 Increased nutrient import from diapycnal mixing

We first explore the possibility that high LLIG bottom-water nutrient concentration in the Florida Straits could have been the result of changes in ocean mixing and argue that this is unlikely to have been the case. The upward mixing of high-nutrient abyssal waters is currently a major source of nutrients to the surface (Fripiat et al., 2021), and a change in the rate of this mixing could explain our results. Little evidence exists referring to a difference in tidal mixing (which is the main driver of the incorporation of deep waters into the upper ocean) between the Late LIG and the Late Holocene. However, sea level was higher throughout the LIG than the Holocene (Veeh, 1966). This would mean the area of underwater continental shelves would have been more expansive in the LIG, and thus more tidal mixing would take place in these shallow regions than in the deep ocean. The opposite trend has been used to explain greater deep mixing during the Last Glacial Maximum (LGM; ca. 20 kyr BP) (*e.g.,* Egbert et al., 2004; Green et al., 2009), driven by sea levels approximately 100 m below the modern. We assume, based on marginally higher sea levels during the Late LIG than the Late Holocene, a similar degree of vertical mixing between the deep and intermediate ocean. Furthermore, a benthic foraminiferal

Cd/Ca record from the deep South Atlantic shows very similar averages for the LIG and the Holocene, suggesting Atlantic deep water Cd_w was comparable during these periods (Oppo and Rosenthal 1994). Thus, the similar degree of vertical mixing coupled with unchanged deep nutrient levels likely did not give rise to an increase in the amount of nutrients mixed upward in the LIG.

4.2 Increased remineralization in the water column

We now consider whether the high LLIG nutrient concentration in the Florida Straits was a result of stronger remineralization and again find that this is not the likely mechanism.

The nutrient load of the intermediate and deep waters that feed the tropical surface ocean can be divided into 'preformed' and 'remineralized' components. Preformed nutrients are present in their dissolved, ionic form in the water mass upon formation, and in the case of the intermediate and deep waters characteristic of the tropical Atlantic, this formation takes place in the North Atlantic or the Southern Ocean. Nutrient concentration in the water mass formation region, and thus preformed nutrient concentration, is determined by the ratio of surface nutrient utilization to nutrient supply in the formation region. This ratio is controlled by an array of factors including (but not limited to) sea ice cover, surface water residence times, and terrigenous dust delivery (Boyd et al., 2001; Robinson et al., 2005). When surface nutrient utilization increases at a rate slower than the concomitant increase in nutrient supply to the surface, the fraction of surface nutrient utilization (that is, nutrients consumed divided by nutrients supplied) decreases, and preformed nutrients increase, as more nutrients remain in the water mass as it mixes into the interior.

Remineralized nutrients are released into the water mass throughout its time in the ocean interior via the decomposition of biomatter. The remineralized component of nutrients in a water mass may change due to a difference in the biomatter rain rate from the surface, or an alteration in the speed or path of the lower ocean water mass; all of these factors could change the total quantity of biomatter available for respiration, as well as the chemical pathway through which that matter is respired (Deutsch & Weber, 2012, and references therein), thereby impacting the quantities of dissolved, ionic nutrients released by remineralization.

Because the cores studied herein were collected on the Bahamas side of the Florida Straits, and the modern mixing of Subantarctic Mode Water and Northern Component Water occurs at

this location (among others in the North Atlantic) (Xu et al., 2022), we can use this data to understand both changes in endmember properties and the mixing regime of NCW and SAMW. Compared to SAMW, NCW is a water mass with moderately higher oxygen (approx. 180 μmol kg^{-1}; Xu et al., 2022), similar temperature (roughly 10°C), similar salinity (roughly 35 psu), and lower nutrient content than SAMW. On the other hand, SAMW is a part of the southern-sourced waters that contribute to the upper limb of the Atlantic Meridional Overturning Circulation and is instrumental in the northward flux of nutrient-replete, cool, low oxygen (approx. 140 μmol kg^{-1}; Xu et al., 2022), low salinity waters from the Antarctic and Subantarctic Zones of the Southern Ocean to the North Atlantic.

Heightened remineralization in NCW and/or SAMW upstream of the Florida Straits in the Late LIG relative to the Late Holocene would increase the nutrient contents of these water masses, thus causing an increase in the nutrient supply to the Florida Straits during the LLIG, which could explain our results. An increase in aerobic remineralization would also necessitate greater oxygen utilization in the water masses before they reach KNR166-2-GGC73/JPC80, however our calculated AOU is only slightly higher in the Late LIG than in the Late Holocene: our estimate for LLIG AOU is 13.3 μmol kg^{-1} (1σ = 34.3 μmol kg^{-1}) greater than our estimate for LH AOU. When applied to the Redfield Ratio for O_2:P (which we take as -170:1), we calculate a maximum (see *Methods*) difference in P_{remin} of 0.078 ± 0.202 μmol kg^{-1} between the LH and the LLIG. Considering our estimates of average [PO_4^{3-}] in the LLIG and LH, we infer that changes in biological remineralization can account for 15 ± 38% of the measured change in Cd_w. This non-negligible signal (with an error spanning 0) indicates that another mechanism is likely responsible for most of the change in Cd_w that we reconstruct. Furthermore, an increase in remineralized nutrients during the LLIG is consistent with increased preformed nutrients as preformed nutrients in intermediate waters fuel tropical surface productivity (Sarmiento et al., 2004), which rains biomatter that is respired in the ocean interior, ultimately producing remineralized nutrients in those same intermediate waters. By this mechanism, preformed nutrients are transformed into remineralized nutrients, and so an increase in preformed nutrients would lead to a rise in remineralized nutrients, as well (Palter et al., 2010).

4.3 Altered Last Interglacial AMOC

We now consider whether changes in AMOC could have produced the higher LLIG nutrient concentrations and again suggest that this hypothesis is insufficient to explain our results. As stated above, because of the role of SAMW in the upper limb of AMOC, its prevalence throughout the North Atlantic is tied to the production of North Atlantic Deep Water (NADW): when NADW production is great (strong AMOC), compensatory northward SAMW flow is great, and vice versa (Bryden et al., 2011). So, when AMOC is strong, SAMW will account for a greater fraction of the water bathing the Florida Straits core site, while when AMOC is weak, NCW will dominate the bottom water of this core site. These changes in Florida Straits bottom water are evident in past reconstructions of nutrient concentration through the last deglaciation (Valley et al., 2017), dissolved oxygen through the Younger Dryas (ca. 12 kyr BP; Lynch-Stieglitz et al., 2024), and temperature through the LGM (Valley et al., 2019). If AMOC had been significantly stronger during the LLIG than during the LH, more SAMW would have been imported into the North Atlantic. Under this scenario, the properties at the bottom of the Florida Straits and the location of KNR166-2-GGC73/JPC80 would have been closer to those of SAMW than NCW. As SAMW is the nutrient-rich endmember, an AMOC strengthening could have increased the nutrient supply to KNR166-2-GGC73/JPC80, so it is conceivable that this could explain the reconstructed Cd_w enrichment during the LLIG.

Conversely, a weaker AMOC state during the LLIG could also be a possible explanation for the Cd_w enrichment. A weaker AMOC state would cause a slowing of the geostrophic flow through the Florida Straits (Weiffenbach et al., 2023), meaning the SAMW, which under strong AMOC conditions primarily abuts the western side of the Straits, would disperse eastward, causing the slopes of the isopycnals spanning the Straits to flatten. This change in isopycnal steepness is evident in the fossil record during events when AMOC is presumed to be weaker than today, such as the Younger Dryas (Lynch-Stieglitz et al., 1994; Lynch-Stieglitz et al., 2024). As KNR166-2-GGC73/JPC80 is on the opposite side of the Florida Straits from the center of the SAMW tongue in the region (Xu et al., 2022), a weakening of AMOC would cause the horizontal extent of the SAMW tongue to grow in the direction of KNR166-2-GGC73/JPC80. Thus, due to the weakened tilt alone–and not considering any change in the amount of SAMW in the region–a weakening of AMOC during the LLIG relative to the LH could also increase the

fraction of southern-sourced water at this core site, thus explaining the difference in Cd_w between these periods.

However, it does not appear that the LLIG AMOC was significantly different from its Late Holocene state. Böhm et al. (2015) presented records of εNd and $^{231}Pa/^{230}Th$ from the deep Bermuda Rise which extend from the present to MIS 6. According to these records, mean $^{231}Pa/^{230}Th$ is identical during the LH (μ = 0.056, n = 10) and the LLIG (μ = 0.056, n = 9), indicating deep water flow speed was similar during these two periods, one sign that AMOC was not significantly different (Böhm et al., 2015). εNd is also similar on average between the LLIG (μ = -13.19, n = 10) and the LH (μ = -14.05, n = 6). Furthermore, the records of LLIG foraminifera and diatom assemblages from the Nordic Seas presented by Ezat et al. (2024) indicate that AMOC-driven freshwater export during the LLIG was extremely similar to the Holocene average, suggesting similar AMOC activity. This notion of similar AMOC strength in the LLIG and the LH is also largely supported by records of benthic $\delta^{13}C$ in the Nordic Sea overflow and the deep Caribbean Sea developed by Galaasen et al. (2014, 2020) and Oppo & Fairbanks (1990), respectively, although these records suggest a marginally weaker AMOC state in the LLIG than the LH. Finally, Guihou et al. (2011) developed records of $^{231}Pa/^{230}Th$ in a North Atlantic depth transect to show high agreement in AMOC state between the LIG and the Holocene. In light of these records, we conclude that the available evidence suggests the ratio of southern-sourced to northern-sourced waters in the Florida Straits was similar during the LLIG and the LH. Thus, we reject the AMOC hypothesis as a primary explanation for our observed increase in nutrient supply to the Florida Straits core site.

4.4 Increased preformed nutrients in endmembers of mixing

In the absence of large changes in regenerated nutrient content or the mixing ratio of SAMW and NCW in the Florida Straits, we turn to a change in the preformed nutrient load of one or both endmembers of mixing to explain the observed variation in Cd_w between the LLIG and the LH.

4.4.1 P_{pre} enrichment in the LLIG Atlantic

First, we examine a record of North Atlantic surface productivity during the LLIG and find that the little existing evidence indicates NCW P_{pre} may not have differed substantially during the LLIG and the LH. Thibodeau et al. (2017) presented a record of bulk sedimentary $\delta^{15}N$ in the

polar North Atlantic. $\delta^{15}N$ is a tracer of nutrient utilization such that lower $\delta^{15}N$ suggests a poorer degree of nitrate consumption by primary producers, resulting in a more abundant supply of dissolved nitrate, which is conducive to greater kinetic fractionation of nitrogen isotopes during nitrate assimilation. This polar record shows a decrease of <1‰ from the LH to the LLIG, indicating little to no difference in nutrient utilization between these periods. These surface waters contribute to the deep winter mixed layer in the subpolar North Atlantic which forms Subpolar Mode Water, which is the principal component of NCW at our core site, according to the local bottom water density of $\sigma_0 \approx 27.0$ kg m^{-3}. The other water masses which we recognize could contribute to NCW, Mediterranean Water and North Atlantic Central Water, both currently form from low-nutrient surface waters, so we assume the preformed nutrient fractions therein were not different during the LLIG. Thus, the record of Thibodeau et al. (2017) supports similar P_{pre} in the northern-sourced endmember of mixing in the Florida Straits during the LLIG. So, we invoke a change in P_{pre} of SAMW to explain the higher Cd_w observed in the Florida Straits during the LLIG.

There is evidence from the region where SAMW forms which supports higher preformed nutrients in this water mass. While few studies focusing on primary productivity in the Southern Ocean have explicitly discussed differences in biogeochemistry between the LLIG and the LH, many published records do capture both of these periods, and they show appreciable changes in factors such as $\delta^{15}N$ and biogenic opal flux in regions important to SAMW formation, specifically the Antarctic Zone (AZ) and the Subantarctic Zone (SAZ). The AZ is where primary productivity takes place in the surface waters that form SAMW before these waters mix downward in the wintertime SAZ to form SAMW. Robinson and Sigman (2008) presented records of diatom-bound $\delta^{15}N$ and $\delta^{18}O_{opal}$ from an Atlantic sediment core in the AZ. These records point to lower $\delta^{15}N$ (poorer nutrient utilization) and higher $\delta^{18}O_{opal}$ (denser surface water) during the LLIG than the LH. Furthermore, a biogenic opal flux record from the Atlantic AZ demonstrates higher export productivity during the LLIG than the LH (Jaccard et al., 2013). The $\delta^{18}O_{opal}$ record indicates an increase in surface density in the AZ during the LLIG relative to the LH, arguing for decreased surface isolation and thus lower residence time of the upper Southern Ocean. Lower surface residence time would hinder the ability of primary producers to consume the nutrient supply from upwelling to completion before the water mass leaves the photic zone. A lower surface residence time might also decrease the degree of oxygen saturation and lead to

577 an overestimation of P_{remin} when calculated using AOU (Ito et al., 2004). With a lower degree of
578 nutrient utilization would come a greater concentration of dissolved nutrients left in the surface
579 waters as the SAMW forms (*i.e.,* greater P_{pre}). Broader LLIG biogenic opal deposition (Jaccard
580 et al., 2013) bolsters this conclusion, revealing that the downturn in nutrient utilization was not
581 driven by lower absolute productivity in the LLIG relative to the LH, but rather an increase in the
582 surface nutrient supply and/or a decrease in the surface residence time.
583 Evidence from the SAZ, where SAMW last sees the surface before mixing downward, does
584 not directly support or refute these conclusions. For instance, Martínez-García et al. (2014)
585 developed records of iron flux, foraminifera-bound $\delta^{15}N$, and alkenone flux from the Atlantic
586 SAZ, and found a roughly 0.5‰ enrichment in $\delta^{15}N$ during the LLIG relative to the LH, with
587 little change in alkenone flux (an export productivity proxy based on the deposition of
588 biomarkers produced by prymnesiophytes). This could indicate that waters leaving the SAZ
589 would have approximately the same P_{pre} in the LLIG as in the LH, disagreeing directly with the
590 preformed nutrients hypothesis. However, Sigman et al. (2021) argued that a change in SAMW
591 P_{pre} could be achieved with changes in nutrient utilization in either the SAZ or the AZ (assuming
592 little change in the other region), or a change in the strength of the upwelling in this region.
593 Hence, the lack of support offered by the limited data from the Atlantic SAZ does not necessarily
594 disprove the preformed nutrients hypothesis.
595
596 *4.4.2 P_{pre} enrichment in the LLIG Indo-Pacific and causes thereof*
597 Evidence of SAMW P_{pre} enrichment during the LLIG is not limited to the Atlantic sector of
598 the Southern Ocean, and in this section, we discuss records from the Indo-Pacific which support
599 this notion and help clarify the mechanism underlying this change in nutrient cycling. Studer et
600 al. (2015) presented records of diatom-bound $\delta^{15}N$, opal flux, and Ba/Fe (another export
601 productivity proxy) from the Pacific sector of the AZ which show approximately equal $\delta^{15}N$
602 during the LLIG and the LH with markedly higher values for opal flux and Ba/Fe during the
603 LLIG. As in the Atlantic records, these records indicate that greater absolute productivity was
604 required to achieve a similar (or poorer) level of nutrient consumption in the AZ during the
605 LLIG, which suggests that the nutrient supply to the surface was greater then, that the surface
606 residence time was shorter, and thus that the absolute quantity of nutrients left unconsumed
607 during water mass formation (*i.e.,* preformed nutrients) was greater in the LLIG.

Furthermore, Ai et al. (2024) used a meridional transect of cores in the South Indian Ocean to indicate that the latitudes of Antarctic Circumpolar Current (ACC) fronts were up to 2° poleward of their Holocene averages during the LLIG. Numerous climate models and reconstructions of past climate conditions (*e.g.*, Barnes & Polvani, 2013; Gray et al., 2023) suggest that a close relationship exists between the latitudes of ACC fronts and that of the Southern Westerly Winds (SWW), such that a poleward shift in one occurs concomitantly with a poleward shift of similar magnitude in the other. Furthermore, these same climate models indicate that the latitude of the SWW is tightly correlated to the strength of the SWW, such that a poleward shift in the SWW is coincident with a strengthening of the SWW (Gray et al., 2023). While the magnitude of the shift in ACC latitude that Ai et al. (2024) reconstructed may not have been homogeneous across the Indian, Pacific, and Atlantic sectors of the Southern Ocean, little evidence of ACC front paleolatitude exists in the Atlantic through the LLIG, so we still take this estimate as a reflection of the direction of change in the Atlantic at the same time. We use this poleward shift in ACC latitude with the aforementioned relationships between ACC latitude and SWW latitude, and between SWW latitude and SWW strength, to infer that, during the LLIG, the SWW were farther poleward and thus stronger. This would have two direct impacts on the Southern Ocean system: 1) strengthening of the ACC; and 2) reinforcement of Ekman upwelling, resulting in a greater rate of overturning. Lamy et al. (2024) used sedimentary sortable silt fractions from sediment cores in the Pacific sector of the Southern Ocean to reconstruct ACC strength and found that the ACC was upwards of 20% stronger during the LLIG than its LH average. Furthermore, the record of greater $\delta^{18}O_{opal}$ in the Atlantic AZ during the LLIG (Robinson & Sigman, 2008) suggests poorer surface stratification, possibly driven by stronger Ekman upwelling. If the ACC was stronger and surface stratification weaker in the LLIG than the LH, we suggest that a poleward shift in the SWW was ultimately responsible for the increase in SAMW P_{pre}.

Our evidence supports the hypothesis that low axial tilt could drive upwelling in the Southern Ocean. Ai et al. (2020) explained that the large difference they observed between measured, diatom-bound $\delta^{15}N$ in the Indian AZ and predicted $\delta^{15}N$ (from a model based on Antarctic air T) in the LLIG is due to this obliquity-driven mode of upwelling. In the LLIG, obliquity was lower than the LH (Berger and Loutre, 1991), which could have led to a steepening of the low-to-high latitude T gradient and thus a strengthening of the SWW and the Ekman upwelling these winds drive during the LLIG. This mechanism facilitated upwelling despite Antarctic cooling across

639 the LLIG (Jouzel et al., 2007), which would have otherwise forced ACC fronts (and the SWW)
640 equatorward and weakened the ACC and SWW. As Ai et al. (2020) note, the Late Holocene is
641 also marked by declining obliquity, but average obliquity is still greater than the LLIG, allowing
642 for a weaker mid-to-high latitude T gradient and inferior upwelling during the LH relative to the
643 LLIG, despite warmer Antarctic temperatures in the LH.
644
645 *4.4.3 Higher equatorial surface productivity during the LLIG*
646 As stated in the introduction, several studies have suggested that, during the LLIG, surface
647 productivity was higher than the Late Holocene in equatorial regions in the Atlantic, Pacific, and
648 Indian Oceans (Piacsek et al., 2021; Marcantonio et al., 2020; Kawahata et al., 1998; Tangunan
649 et al., 2017; Romero et al., 2012). The cores from which these productivity records were
650 developed all underlie surface waters within the circumequatorial band of Si* from -10 μmol kg^{-1}
651 to -15 μmol kg^{-1} (defined as the difference between concentrations of silicic acid and nitrate;
652 Sarmiento et al., 2004); this range is characteristic of SAMW, implying that SAMW nutrient
653 content modulates surface productivity at these sites (Sarmiento et al., 2004). The relationship
654 between SAMW nutrient concentration and equatorial productivity–including changes in the
655 Southern Westerly Winds serving as a driving mechanism for change in SAMW P_{pre}–has been
656 inferred from modern SAMW trends and the shifts in equatorial productivity with which they
657 correlate well (Ayers & Strutton, 2013). Almost all of the equatorial productivity records we cite
658 include age models developed from radiocarbon and planktonic foraminiferal $\delta^{18}O$, so we argue
659 that incongruity in age models is not a challenge to the explanation of LLIG changes in these
660 equatorial cores using data from the reconstructions we generated.
661 Due to the paucity of records of intermediate water nutrient concentration that resolve the
662 LLIG, records that describe higher equatorial productivity during the LLIG than the LH could
663 previously only be explained by inference (that is, under the substantiated assumption that light
664 and micronutrient delivery were not limiting productivity during the LLIG; see *Introduction)*.
665 Now, our records indicate that these reconstructed increases in equatorial productivity may be
666 attributable to the increase in SAMW preformed nutrients that we infer.
667
668 ## *5. Conclusions*
669

We presented new records of temperature, seawater cadmium concentration, and bottom-water dissolved oxygen content from the Bahamas side of the Florida Straits. We observe that, in the Late Last Interglacial, Cd_w was substantially higher than the average Late Holocene value (a difference of over 60%) with an incongruously small increase in apparent oxygen utilization. The published evidence from an array of sediment cores in the Atlantic (Robinson & Sigman, 2008), Indian (Ai et al., 2024), and Pacific (Lamy et al., 2024; Studer et al., 2015) sectors of the Southern Ocean are consistent with southward-shifted Southern Westerly Winds and Antarctic Circumpolar Current in the LLIG relative to the LH, which would come with a strengthening of these atmospheric and oceanic currents. With a strengthening in SWW would come an increase in Ekman upwelling in the Southern Ocean, which would decrease surface residence time and increase the nutrient supply to the photic layer, assuming a relatively constant level of nutrients in the deep waters mixing upward there (Oppo and Rosenthal, 1994). Such changes led to a decrease in the degree of nutrient consumption and an increase in the nutrient load borne by the surface waters as they mixed downward in the Subantarctic Zone to form Subantarctic Mode Water. Thus, we propose that higher preformed phosphate in SAMW during the LLIG was responsible for much of the change in Florida Straits Cd_w we reconstruct.

Due to the impact of SAMW nutrient concentration on tropical productivity (Sarmiento et al., 2004), we also attribute previously unexplained increases in equatorial productivity observed in the Atlantic (Piacsek et al., 2021), Pacific (Marcantonio et al., 2020), and Indian (Romero et al., 2012; Tangunan et al., 2017) Oceans during the Late Last Interglacial to the increase in SAMW preformed nutrients.

Data Availability:

The novel data used to draw the conclusions in this paper are archived in the PANGAEA database (Sipp-Alpers et al., 2025).

Conflict of Interest Statement:

The authors declare that they have no conflicts of interest according to affiliations or funding which could influence the contents of this work.

Acknowledgements:

The authors would like to thank S. Wang and W. Lu for providing previously unpublished trace metal data; K. Thirumalai and A. Manoogian for the development of replicate isotopic measurements on *Globobulimina spp.*; B. Buyurgan for assistance with age model software; L. van Maldegem for assistance in the INSTAAR Trace Metal Lab; D. Sigman and I. Bolden for helpful discussions; and two anonymous reviewers for their helpful comments. This work was supported by the Georgia Tech School of Earth & Atmospheric Sciences Rutt Bridges Undergraduate Research Award and by U.S. National Science Foundation Grants OCE-1851900 to Lynch-Stieglitz and OCE-2233080 to Marchitto.

References

Ai, X. Y. E., Studer, A. S., Sigman, D. M., Martínez-García, A., Fripiat, F., Thöle, L. M., et al. (2020). Southern Ocean upwelling, Earth's obliquity, and glacial-interglacial atmospheric CO change. *Science, 370*(6522), 1348-+.

Ayers, J. M., & Strutton, P. G. (2013). Nutrient variability in Subantarctic Mode Waters forced by the southern annular mode and ENSO. *Geophysical Research Letters, 40*(13), 3419–3423.

Anderson, L. A., & Sarmiento, J. L. (1994). Redfield Ratios of Remineralization Determined by Nutrient Data-Analysis. *Global Biogeochemical Cycles, 8*(1), 65-80.

Barnes, E. A., & Polvani, L. M. (2013). Response of the midlatitude jets, and of their variability, to increased greenhouse gases in the CMIP5 models. *Journal of Climate, 26*(18), 7117–7135.

Barnett, R. L. et al. (2023). Constraining the contribution of the Antarctic Ice Sheet to Last Interglacial sea level. *Sci. Adv.* 9, eadf0198.

Berger, A., & Loutre, M. F. (1991). Insolation Values for the Climate of the Last 10000000 Years. *Quaternary Science Reviews, 10*(4), 297-317.

Bohm, E., Lippold, J., Gutjahr, M., Frank, M., Blaser, P., Antz, B., et al. (2015). Strong and deep Atlantic meridional overturning circulation during the last glacial cycle. *Nature, 517*(7532), 73-U170.

Bova, S., Rosenthal, Y., Liu, Z. Y., Godad, S. P., & Yan, M. (2021). Seasonal origin of the thermal maxima at the Holocene and the last interglacial. *Nature, 589*(7843), 548-+.

Boyle, E., Sclater, F. & Edmond, J. (1976). On the marine geochemistry of cadmium. *Nature* **263**, 42–44.

Boyle, E. A. (1983). Manganese carbonate overgrowths on foraminifera tests. *Geochimica et Cosmochimica Acta, 47*, 1815-1819.

Boyle, E. A. (1992). Cadmium and $\delta^{13}C$ paleochemical ocean distributions during the Stage 2 glacial maximum. *Annual Review of Earth and Planetary Sciences, 20*, 245-287.

Boyle, E. A., Labeyrie, L., & Duplessy, J. C. (1995). Calcitic Foraminiferal Data Confirmed by Cadmium in Aragonitic Hoeglundina - Application to the Last Glacial Maximum in the Northern Indian-Ocean. *Paleoceanography, 10*(5), 881-900.

Boyle, E. A., & Rosenthal, Y. (1996). Chemical hydrography of the South Atlantic during the Last Glacial Maximum: Cd vs. $\delta^{13}C$. In G. Wefer, W. H. Berger, G. Siedler, & D. Webb (Eds.), *The South Atlantic: Present and Past Circulation* (pp. 423–443). Springer, Berlin, Heidelberg.

Brandt, P., Körner, M., Moum, J. N., et al. (2025). Seasonal productivity of the equatorial Atlantic shaped by distinct wind-driven processes. *Nature Geoscience, 18*, 84-90.

Bryan, S. P., & Marchitto, T. M. (2008). Mg/Ca-temperature proxy in benthic foraminifera: New calibrations from the Florida Straits and a hypothesis regarding Mg/Li. *Paleoceanography, 23*(2).

Bryan, S. P., & Marchitto, T. M. (2010). Testing the utility of paleonutrient proxies Cd/Ca and Zn/Ca in benthic foraminifera from thermocline waters. *Geochemistry Geophysics Geosystems, 11*.

Bryden, H. L., King, B. A., & McCarthy, G. D. (2011). South Atlantic overturning circulation at 24°S. *Journal of Marine Research, 69*(1), 39-56.

Costa, K. M., Jacobel, A. W., McManus, J. F., Anderson, R. F., Winckler, G., & Thiagarajan, N. (2017). Productivity patterns in the equatorial Pacific over the last 30,000 years. *Global Biogeochemical Cycles, 31*(5), 850-865.

Deutsch, C., & Weber, T. (2012). Nutrient Ratios as a Tracer and Driver of Ocean Biogeochemistry. *Annual Review of Marine Science, Vol 4, 4*, 113-+.

Egbert, G. D., R. D. Ray, and B. G. Bills (2004), Numerical modeling of the global semidiurnal tide in the present day and in the last glacial maximum, *J. Geophys. Res., 109*, C03003.

Eggleston, S., Schmitt, J., Bereiter, B., Schneider, R., & Fischer, H. (2016). Evolution of the stable carbon isotope composition of atmospheric CO_2 over the last glacial cycle. *Paleoceanography, 31*(3), 434-452.

Elderfield, H., & Rickaby, R. E. M. (2000). Oceanic Cd/P ratio and nutrient utilization in the glacial Southern Ocean. *Nature, 405*(6784), 305-310.

Ezat, M. M., Fahl, K., & Rasmussen, T. L. (2024). Arctic freshwater outflow suppressed Nordic Seas overturning and oceanic heat transport during the Last Interglacial. *Nature Communications, 15*(1).

Fripiat, F., Martínez-García, A., Marconi, D., Fawcett, S. E., Kopf, S. H., Luu, V. H., et al. (2021). Nitrogen isotopic constraints on nutrient transport to the upper ocean. *Nature Geoscience, 14*(11), 855-+.

Galaasen, E. V., et al. (2014). Rapid reductions in North Atlantic Deep Water during the peak of the last interglacial period. *Science, 343*, 1129-1132.

Galaasen, E. V., et al. (2020). Interglacial instability of North Atlantic Deep Water ventilation. *Science, 367*, 1485-1489.

Gray, W. R., de Lavergne, C., Wills, R. J. C., Menviel, L., Spence, P., Holzer, M., et al. (2023). Poleward Shift in the Southern Hemisphere Westerly Winds Synchronous With the Deglacial Rise in CO_2. *Paleoceanography and Paleoclimatology, 38*(7).

Green, J. A. M., C. L. Green, G. R. Bigg, T. P. Rippeth, J. D. Scourse, and K. Uehara (2009), Tidal mixing and the Meridional Overturning Circulation from the Last Glacial Maximum, Geophys. Res. Lett., 36, L15603.

Guihou, A., Pichat, S., Govin, A., Nave, S., Labeyrie, L., Michel, E., Duplessy, J.-C., Telouk, P., & Waelbroeck, C. (2011). Enhanced Atlantic Meridional Overturning Circulation supports the Last Glacial Inception. *Quaternary Science Reviews, 30*(13-14), 1576–1582.

Hoffman, J. S., Clark, P. U., Parnell, A. C., & He, F. (2017). Regional and global sea-surface temperatures during the last interglaciation. *Science, 355*(6322), 276-279.

Hoogakker, B. A. A., Elderfield, H., Schmiedl, G., McCave, I. N., & Rickaby, R. E. M. (2015). Glacial-interglacial changes in bottom-water oxygen content on the Portuguese margin. *Nature Geoscience, 8*(1), 40-43.

Hoogakker, B. A. A., et al. (2025). Review of proxies for low-oxygen paleoceanographic reconstructions. *Biogeosciences, 22*, 863-957.

Ito, T., Follows, M. J., & Boyle, E. A. (2004). Is AOU a good measure of respiration in the oceans? *Geophysical Research Letters, 31*(17).

Jaccard, S. L., Hayes, C. T., Martínez-García, A., Hodell, D. A., Anderson, R. F., Sigman, D. M., & Haug, G. H. (2013). Two Modes of Change in Southern Ocean Productivity Over the Past Million Years. *Science, 339*(6126), 1419-1423.

Jacobel, A. W., McManus, J. F., Anderson, R. F., & Winckler, G. (2017). Climate-related response of dust flux to the central equatorial Pacific over the past 150 kyr. *Earth and Planetary Science Letters, 457*, 160-172.

Johnson, G. C. (2008). Quantifying Antarctic Bottom Water and North Atlantic Deep Water volumes. *Journal of Geophysical Research, 113*, C05027.

Jouzel, J., Masson-Delmotte, V., Cattani, O., Dreyfus, G., Falourd, S., Hoffmann, G., et al. (2007). Orbital and millennial Antarctic climate variability over the past 800,000 years. *Science, 317*(5839), 793-796.

Karstensen, J., Stramma, L., & Visbeck, M. (2008). Oxygen minimum zones in the eastern tropical Atlantic and Pacific oceans. *Progress in Oceanography, 77*(4), 331–350.

Kawahata, H., Suzuki, A., & Ahagon, N. (1998). Biogenic sediments in the West Caroline Basin, the western equatorial Pacific during the last 330,000 years. *Marine Geology, 149*(1–4), 155–176.

Kohfeld, K. E., & Chase, Z. (2017). Temporal evolution of mechanisms controlling ocean carbon uptake during the last glacial cycle. *Earth and Planetary Science Letters, 472*, 206–215.

Lamy, F., Winckler, G., Arz, H. W., Farmer, J. R., Gottschalk, J., Lembke-Jene, L., et al. (2024). Five million years of Antarctic Circumpolar Current strength variability. *Nature, 627*(8005).

Leduc, G., Schneider, R., Kim, J. H., & Lohmann, G. (2010). Holocene and Eemian sea surface temperature trends as revealed by alkenone and Mg/Ca paleothermometry. *Quaternary Science Reviews, 29*(7-8), 989-1004.

Lee, T., Rand, D., Lisiecki, L. E., Gebbie, G., & Lawrence, C. (2023). Bayesian age models and stacks: combining age inferences from radiocarbon and benthic $\delta^{18}O$ stratigraphic alignment. *Climate of the Past, 19*(10), 1993-2012.

Little, S. H., Vance, D., Lyons, T. W., & McManus, J. (2015). Controls on trace metal authigenic enrichment in reducing sediments: Insights from modern oxygen-deficient settings. *American Journal of Science*, *315*(2), 77–119.

Lisiecki, L. E., & Raymo, M. E. (2005). A Pliocene-Pleistocene stack of 57 globally distributed benthic $\delta^{18}O$ records -: art. no. PA1003. *Paleoceanography, 20*(1).

Lisiecki, L. E. (2010). A simple mixing explanation for late Pleistocene changes in the Pacific-South Atlantic benthic $\delta^{13}C$ gradient. *Climate of the Past, 6*, 305-314.

Lisiecki, L. E., & Stern, J. V. (2016). Regional and global benthic δ ^{18}O stacks for the last glacial cycle. *Paleoceanography, 31*(10), 1368-1394.

Lu, W. Y., Guo, W. F., & Oppo, D. W. (2024). Assessing the Precision and Accuracy of Foraminifera Elemental Analysis at Low Ratios. *Geochemistry Geophysics Geosystems, 25*(10).

Lutze, G. F., & Thiel, H. (1989). Epibenthic foraminifera from elevated microhabitats: *Cibicidoides wuellerstorfi* and *Planulina ariminensis*. *Journal of Foraminiferal Research*, *19*, 153-158.

Lynch-Stieglitz, J., Curry, W. B., & Slowey, N. (1999). Weaker Gulf Stream in the Florida straits during the last glacial maximum. *Nature, 402*(6762), 644-648.

Lynch-Stieglitz, J., W. B. Curry, and D. C. Lund (2009), Florida Straits density structure and transport over the last 8000 years, *Paleoceanography*, *24*, PA3209,

Lynch-Stieglitz, J., Schmidt, M. W., & Curry, W. B. (2011). Evidence from the Florida Straits for Younger Dryas ocean circulation changes. *Paleoceanography, 26*.

Lynch-Stieglitz, J. and T. Marchitto, Tracers of past ocean circulation. (2014). In Holland H.D. and Turekian K.K. (eds.), Treatise on Geochemistry, second edition. Oxford: Elsevier, vol. 8, pp. 435-451.

Lynch-Stieglitz, J., Vollmer, T. D., Valley, S. G., Blackmon, E., Gu, S. F., & Marchitto, T. M. (2024). A diminished North Atlantic nutrient stream during Younger Dryas climate reversal. *Science, 384*(6696), 693-696.

Lynch-Stieglitz, J., & Fairbanks, R. G. (1994). Glacial-Interglacial History of Antarctic Intermediate Water - Relative Strengths of Antarctic Versus Indian-Ocean Sources. *Paleoceanography, 9*(1), 7-29.

Marcantonio, F., Hostak, R., Hertzberg, J. E., & Schmidt, M. W. (2020). Deep Equatorial Pacific Ocean Oxygenation and Atmospheric CO_2 Over The Last Ice Age. *Scientific Reports, 10*(1).

Marchitto, T., Curry, W. & Oppo, D. (1998). Millennial-scale changes in North Atlantic circulation since the last glaciation. *Nature* **393**, 557–561.

Marchitto, T. M. (2006). Precise multielemental ratios in small foraminiferal samples determined by sector field ICP-MS. *Geochemistry Geophysics Geosystems, 7*.

858 Marchitto, T. M., Oppo, D. W., & Curry, W. B. (2002). Paired benthic foraminiferal Cd/Ca and
859 Zn/Ca evidence for a greatly increased presence of Southern Ocean Water in the glacial
860 North Atlantic. *Paleoceanography, 17*(3).
861 Marchitto, T. M., Lynch-Stieglitz, J., & Hemming, S. R. (2005). Deep Pacific $CaCO_3$
862 compensation and glacial-interglacial atmospheric CO_2. *Earth and Planetary Science*
863 *Letters, 231*(3-4), 317-336.
864 Marchitto, T. M., Bryan, S. P., Doss, W., McCulloch, M. T., & Montagna, P. (2018). A simple
865 biomineralization model to explain Li, Mg, and Sr incorporation into aragonitic
866 foraminifera and corals. *Earth and Planetary Science Letters, 481*, 20–29.
867 Marcott, S. A., Shakun, J. D., Clark, P. U., & Mix, A. C. (2013). A Reconstruction of Regional
868 and Global Temperature for the Past 11,300 Years. *Science, 339*(6124), 1198-1201.
869 Martínez-García, A., et al. (2014). Iron fertilization of the Subantarctic Ocean during the last ice
870 age. *Science, 343*, 1347-1350.
871 Martrat, B., Grimalt, J. O., Shackleton, N. J., de Abreu, L., Hutterli, M. A., & Stocker, T. F.
872 (2007). Four climate cycles of recurring deep and surface water destabilizations on the
873 Iberian margin. *Science, 317*(5837), 502-507.
874 McCorkle, D. C., Martin, P. A., Lea, D. W., & Klinkhammer, G. P. (1995). Evidence of a
875 dissolution effect on benthic foraminiferal shell chemistry: $\delta^{13}C$, Cd/Ca, Ba/Ca, and
876 Sr/Ca results from the Ontong Java Plateau. *Paleoceanography, 10*(4), 699-714.
877 Middag, R., van Heuven, S. M. A. C., Bruland, K. W., & de Baar, H. J. W. (2018). The
878 relationship between cadmium and phosphate in the Atlantic Ocean unravelled. *Earth*
879 *and Planetary Science Letters, 492*, 79-88.
880 Nascimento, R. A., Shimizu, M. H., Venancio, I. M., Chiessi, C. M., Kuhnert, H., Johnstone, H.
881 J. H., et al. (2022). Warmer western tropical South Atlantic during the Last Interglacial
882 relative to the current interglacial period. *Global and Planetary Change, 215*.
883 Nomaki, H., Chikaraishi, Y., Tsuchiya, M., Toyofuku, T., Suga, H., Sasaki, Y., Ohkouchi, N., et
884 al. (2015). Variation in the nitrogen isotopic composition of amino acids in benthic
885 foraminifera: Implications for their adaptation to oxygen-depleted environments.
886 *Limnology and Oceanography, 60*(1), 1–17.

887 Oppo, D. W., Lu, W., Huang, K. F., Umling, N. E., Guo, W., Yu, J., et al. (2023). Deglacial
888 Temperature and Carbonate Saturation State Variability in the Tropical Atlantic at
889 Antarctic Intermediate Water Depths. *Paleoceanography and Paleoclimatology, 38*(9).
890 Oppo, D. W., & Rosenthal, Y. (1994). Cd/Ca Changes in a Deep Cape Basin Core over the Past
891 730,000 Years - Response of Circumpolar Deep-Water Variability to Northern-
892 Hemisphere Ice-Sheet Melting. *Paleoceanography, 9*(5), 661-675.
893 Oppo, D. W., & Fairbanks, R. G. (1990). Atlantic Ocean thermohaline circulation of the last
894 150,000 years: Relationship to climate and atmospheric CO_2. *Paleoceanography, 5* (3),
895 277-288.
896 Pelejero, C., Grimalt, J. O., Heilig, S., Kienast, M., & Wang, L. J. (1999). High-resolution
897 $U(K)_{37}$ temperature reconstructions in the South China Sea over the past 220 kyr.
898 *Paleoceanography, 14*(2), 224-231.
899 Petit, J. R., Jouzel, J., Raynaud, D., et al. (1999). Climate and atmospheric history of the past
900 420,000 years from the Vostok ice core, Antarctica. *Nature, 399*, 429-436.
901 Piacsek, P., Behling, H., Gu, F., Venancio, I. M., Lessa, D. V. O., Belem, A., & Albuquerque, A.
902 L. S. (2021). Changes in sea surface hydrography and productivity in the western
903 equatorial Atlantic since the last interglacial. *Palaeogeography Palaeoclimatology*
904 *Palaeoecology, 562*.
905 Palter, J. B., Sarmiento, J. L., Gnanadesikan, A., Simeon, J., & Slater, R. D. (2010). Fueling
906 export production: Nutrient return pathways from the deep ocean and their dependence
907 on the Meridional Overturning Circulation. *Biogeosciences, 7*, 3549-3568.
908 Robinson, R. S., & Sigman, D. M. (2008). Nitrogen isotopic evidence for a poleward decrease in
909 surface nitrate within the ice age Antarctic. *Quaternary Science Reviews, 27*(9-10), 1076-
910 1090.
911 Romero, O. E., Mohtadi, M., Helmke, P., & Hebbeln, D. (2012). High interglacial diatom
912 paleoproductivity in the westernmost Indo-Pacific Warm Pool during the past 130,000
913 years. *Paleoceanography, 27*.
914 Roshan, S., & DeVries, T. (2021). Global contrasts between oceanic cycling of cadmium and
915 phosphate. *Global Biogeochemical Cycles, 35*(6), e2021GB006952.
916 Sarmiento, J. L., Gruber, N., Brzezinski, M. A., & Dunne, J. P. (2004). High-latitude controls of
917 thermocline nutrients and low latitude biological productivity. *Nature, 427*(6969), 56-60.

Schlitzer, Reiner, Ocean Data View, https://odv.awi.de, 2023.

Schneider, R.R., Müller, P.J., Ruhland, G., Meinecke, G., Schmidt, H., Wefer, G. (1996). Late Quaternary Surface Temperatures and Productivity in the East-Equatorial South Atlantic: Response to Changes in Trade/Monsoon Wind Forcing and Surface Water Advection. In: The South Atlantic. Springer, Berlin, Heidelberg.

Sigman, D. M., Fripiat, F., Studer, A. S., Kemeny, P. C., Martínez-García, A., Hain, M. P., Ai, X., Wang, X., Ren, H., & Haug, G. H. (2021). The Southern Ocean during the ice ages: A review of the Antarctic surface isolation hypothesis, with comparison to the North Pacific. *Quaternary Science Reviews, 254*, Article 106732.

Sipp-Alpers, I. Lynch-Stieglitz, J. Vollmer, T. Marchitto, T. (2025). Isotopic and trace metal records of benthic foraminifera from Florida Straits sediment cores KNR166-2-JPC80 and KNR166-2-GGC73 [Dataset]. PANGAEA, https://doi.org/10.1594/PANGAEA.985385

Skonieczny, C., McGee, D., Winckler, G., Bory, A., Bradtmiller, L. I., Kinsley, C. W., et al. (2019). Monsoon-driven Saharan dust variability over the past 240,000 years. *Science Advances, 5*(1).

Slowey, N. C., & Curry, W. B. (1995). Glacial-interglacial differences in circulation and carbon cycling within the upper western North Atlantic. *Paleoceanography, 10*, 715-732.

Su, X., Liu, C., Beaufort, L., Barbarin, N., & Jian, Z. (2015). Differences in Late Quaternary primary productivity between the western tropical Pacific and the South China Sea: Evidence from coccoliths. *Deep-Sea Research Part II: Topical Studies in Oceanography*, *122*, 131–141.

Sun, Y., & An, Z. (2005). Late Pliocene-Pleistocene changes in mass accumulation rates of eolian deposits on the central Chinese Loess Plateau. *Journal of Geophysical Research*, *110*, D23101.

Tangunan, D., Baumann, K. H., Pätzold, J., Henrich, R., Kucera, M., De Pol-Holz, R., & Groeneveld, J. (2017). Insolation forcing of coccolithophore productivity in the western tropical Indian Ocean over the last two glacial-interglacial cycles. *Paleoceanography, 32*(7), 692-709.

947 Thibodeau, B., Bauch, H. A., & Pedersen, T. F. (2017). Stratification-induced variations in
948 nutrient utilization in the Polar North Atlantic during past interglacials. *Earth and*
949 *Planetary Science Letters, 457*, 127-135.
950 Tyrrell, T. (2008). Calcium carbonate cycling in future oceans and its influence on future
951 climates. *Journal of Plankton Research, 30*(2), 141-156.
952 Valley, S., Lynch-Stieglitz, J., & Marchitto, T. M. (2017). Timing of Deglacial AMOC
953 Variability From a High-Resolution Seawater Cadmium Reconstruction.
954 *Paleoceanography, 32*(11), 1195-1203.
955 Valley, S. G., Lynch-Stieglitz, J., & Marchitto, T. M. (2019). Intermediate water circulation
956 changes in the Florida Straits from a 35 ka record of Mg/Li-derived temperature and
957 Cd/Ca-derived seawater cadmium. *Earth and Planetary Science Letters, 523*.
958 Veeh, H. H. (1966), Th230/U238 and U234/U238 ages of Pleistocene high sea level stand, J.
959 Geophys. Res., 71(14), 3379–3386.
960 Vollmer, T. D., Ito, T., & Lynch-Stieglitz, J. (2022). Proxy-based preformed phosphate estimates
961 point to increased biological pump efficiency as primary cause of Last Glacial Maximum
962 CO_2 drawdown. *Paleoceanography and Paleoclimatology, 37*, e2021PA004339.
963 Weiffenbach, J. E., Baatsen, M. L. J., Dijkstra, H. A., von der Heydt, A. S., Abe-Ouchi, A.,
964 Brady, E. C., et al. (2023). Unraveling the mechanisms and implications of a stronger
965 mid-Pliocene Atlantic Meridional Overturning Circulation (AMOC) in PlioMIP2.
966 *Climate of the Past, 19*(1), 61-85.
967 Winckler, G., Anderson, R. F., Jaccard, S. L., Marcantonio, F. (2016). Ocean dynamics, not dust,
968 have controlled equatorial Pacific productivity over the past 500,000 years. *PNAS*,
969 *113*(22), 6119-6124.
970 Xu, Y. Y., Wanninkhof, R., Osborne, E., Baringer, M., Barbero, L., Cai, W. J., & Hooper, J.
971 (2022). Inorganic Carbon Transport and Dynamics in the Florida Straits. *Journal of*
972 *Geophysical Research-Oceans, 127*(10).
973